SLAC-PUB-5760
April 1992

A Three-Gap Klystron Output Cavity at X Band

K. Ko et al.

Contributed to the SPIE's Optics, Electro-Optics and Laser Applications in Science and Engineering Symp. (OE/LASE'92), Los Angeles, CA, Jan 19-25, 1992

Stanford Linear Accelerator Center, Stanford University, Stanford, CA 94309

Work supported by Department of Energy contract DE–AC03–76SF00515.

A THREE-GAP KLYSTRON OUTPUT CAVITY AT X-BAND[†]

K. Ko, T.G. Lee, N. Kroll[‡], S. Tonegawa[*]

Stanford Linear Accelerator Center
Stanford University, Stanford, California 94309

ABSTRACT

A high-power X-band klystron employing a double-gap output cavity has been operating at SLAC. Multi-gap output circuits have lower surface gradients at the interaction gaps than single-gap ones but are prone to self-oscillate due to negative beam loading and trapped higher-order modes. In the double-gap circuit design, considerable attention had been directed to deal with these stability problems. The performance of the present tube appears to be limited by gap breakdown and beam interception particularly at long pulses. A three-gap output cavity is currently under development to further reduce the gap surface gradient. Another new feature of the circuit is an enlarged downstream drift tube to improve on beam clearance. This paper discusses the considerations involved in designing a multi-gap output cavity and presents the cold test measurements on the three-gap circuit. The experimental data is compared with numerical results from the 3-D simulation code ARGUS.

I. INTRODUCTION

In developing high peak power klystrons for future linear colliders at high frequencies, a major problem one is confronted with is the high surface gradients in the output circuit due to the small dimensions and the high voltage used. At the Stanford Linear Accelerator Center, there is an ongoing klystron program to generate 100 MW peak power at 11.4 GHz (X-band) with a pulse length of about a microsecond.[1] The first experimental device (XC-1) employed a conventional single-gap output cavity with a calculated maximum surface gradient of 1.3 MV/cm at the 100 MW power level. Severe breakdown and erosion at the output gap were observed. Although work on X-band accelerator structures shows that surface gradients of the order of 5 MV/cm can be sustained for microsecond pulses,[2] the environment in a klystron output circuit is much more severe because of a very high density beam passing through the gap with beam conditions reaching 510 A and 440 KV.

By coupling two gaps through the common wall, a double-gap output cavity was developed and used in the XC-2 klystron, which resulted in an increase in output power. The calculated maximum surface gradient at the gaps is reduced to about 800 KV/cm. In a coupled-cavity chain, there is a potential stability problem because of negative beam loading.[3] Furthermore, self-oscillations due to trapped higher-order (antisymmetric) modes are possible.[4] In the design of the double-gap output circuit, both these issues were addressed.

While the double-gap circuit improved the gap conditions somewhat, the surface gradient reduction is not sufficient to allow the tube to operate at the designed voltage and current for maximum power generation. Gap breakdown remains a limiting factor. So is the power handling capability of the output window which is a topic beyond the scope of the present paper. In principle, the maximum surface gradient decreases as the number of gaps increases, provided that the impedances of the gaps are such that the beam-induced voltage across them are lower. Such a multi-gap circuit is desirable only if a resonably high conversion efficiency can be expected. These two requirements have been the focus of the current effort to develop a three-gap

[†]Work supported by Department of Energy contracts DE-AC03-76SF00515 and AS0-89ER4-527[‡].
[‡]Also at Dept. of Physics, UCSD, La Jolla, Calif.
[*]Currently at NEC Corporation, Kawasaki, Japan.

output cavity to further reduce the surface gradient and to improve on the efficiency. A schematic drawing of the cavity is shown in Figure 1. A single tapered slot couples adjacent cells for a total of two slots and they lie on opposite sides of the vertical symmetry plane. The enlarged drift tube is downstream from the output gap and just before the collector which is not shown.

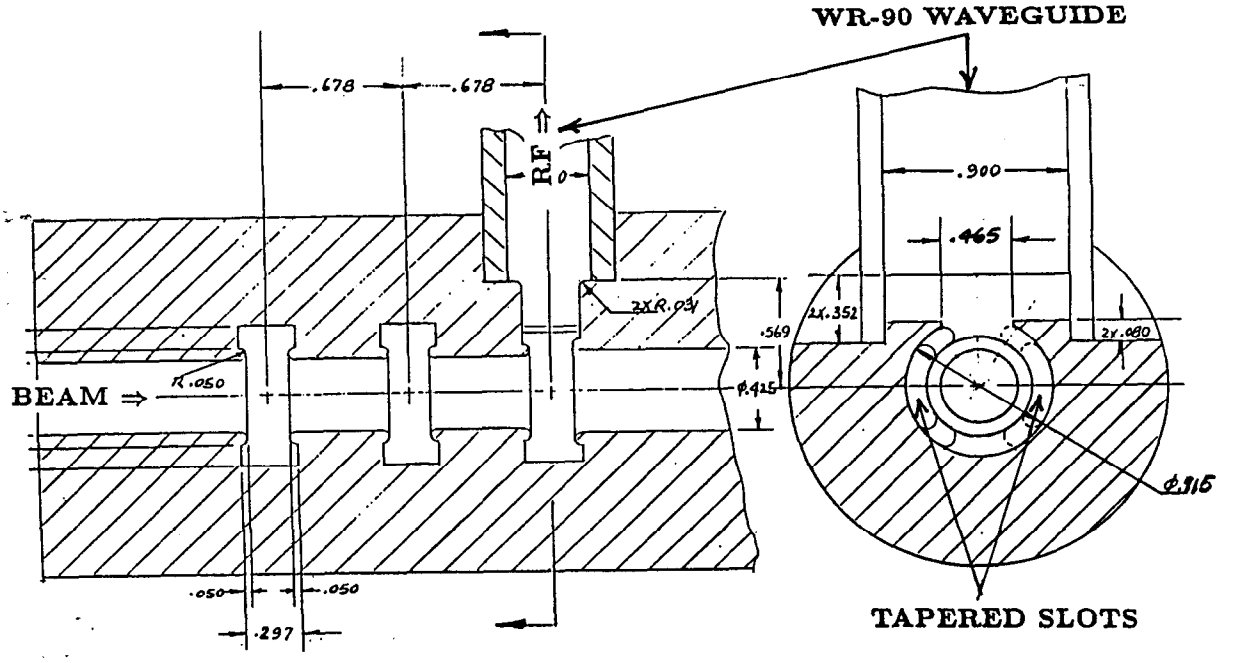

Figure 1. Schematic drawing of the three-gap output cavity.

This paper describes the methodology for designing the three-gap output cavity which in principle, applies to any multi-gap output circuit. First cold test is performed on the prototype circuit to determine the mode spectrum and the external Q of each mode. For the modes in the lowest pass band which are azimuthally symmetric, further experiments are done to measure the impedance of the circuit at each of the mode frequencies. The measurement procedure is based on Zhao's method for a double-gap output cavity[5] and extended here to the three-gap case. From the circuit impedance he shows how the gap impedances can be derived. The circuit conductance obtained from the gap impedances is then compared with the calculated beam loading conductance to provide some indication of any mode instability due to negative beam loading. For modes in the higher pass bands, the cold test data is compared with numerical results from the 3-D electromagnetic code ARGUS[6] to identify trapped modes. One can generate mode patterns more readily on the computer than by experiment. They are useful for studying field asymmetries and for finding ways to load down trapped modes properly. Separately, the gap impedances for the operating 2π mode are used in the $2\frac{1}{2}$-D particle-in-cell code CONDOR[7] to calculate the induced gap voltages as well as the conversion efficiency so that the circuit's performance in the presence of a beam can be evaluated.

In theory, the design procedures outlined above can be iterated until the requirements on a safe surface gradient (below the breakdown threshold) and a reasonable efficiency, are met simultaneously. In practice, however, the two objectives are often not mutually inclusive as the results to date seem to indicate. The present paper reports on the ongoing effort to realize the high power, high frequency three-gap output circuit. Section II summarizes Zhao's method for measuring the circuit impedance matrix as applied to the three-gap case and demonstrates how the gap impedances are derived. Section III treats the negative beam loading issue for the modes in the lowest passband while section IV compares the cold test measurements with ARGUS simulations. Section V shows the gap voltages and the efficiency as calculated by CONDOR using the gap impedances found for the operating mode in the present design. Finally, several concluding remarks are included in section VI.

II. CIRCUIT AND GAP IMPEDANCES

A method of measuring the impedance of a double-gap klystron output cavity was first introduced by Zhao. The extension of his method to the present case of a three-gap output cavity is briefly described in this section. The analysis is based on microwave network theory. The cavity is represented by an equivalent four-port network as shown in Fig. 2.

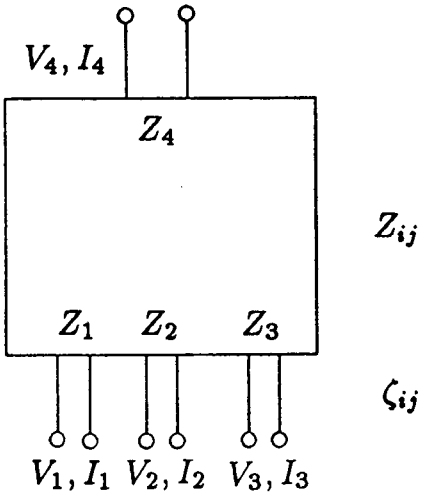

Figure 2. An equivalent four-port microwave network.

Three of the ports correspond to the three gaps while the fourth port refers to the output waveguide. At a given frequency, the voltages and currents at the four ports can be written as follows

$$V_i = \sum_j Z_{ij} I_j \tag{1}$$

with $i, j = 1, .., 4$. Z_{ij} is the circuit impedance that relates the voltage at port i to the current at port j. At port i, one can also write

$$V_i = Z_i I_i \tag{2}$$

where Z_i is now the terminating impedance at that port. From Eqs. (1) and (2), one can solve specifically for the output port impedance Z_4 which, for simplicity, is expressed here in functional form as

$$Z_4 = F(Z_1, Z_2, Z_3; Z_{11}, ..., Z_{44}). \tag{3}$$

It depends on the port impedances and the circuit impedance matrix. The circuit impedance remains fixed for a given design so if Z_1, Z_2, Z_3 are varied, Z_4 will change, which can readily be measured. Now only ten of the elements in the 4x4 impedance matrix are independent so Z_4 is really a function of ten unknowns and three varying parameters. By measuring Z_4 for ten different sets of port impedances which amount to ten different combinations of gap conditions, the matrix can be uniquely determined from the solutions to the coupled set of equations as represented by (3).

Experimentally, the gaps can either be opened (o), shorted (s) or perturbed (p) which corresponds to an impedance of value ∞, 0 or Z_p respectively. Specifically if the perturbation is due to a small metal bead, it is equivalent to an extra capacitance shunting the gap so that Z_p=-1/ $j\omega\Delta C$. In the measurements, Zhao suggested choosing the reference plane at the output port to be at the standing-wave minimum when all the gaps are open. In this case, assuming no loss, the impedance is zero; therefore

$$Z_{44} = 0 \tag{4}$$

Taking this reference plane as the origin, the remaining nine measurements can be expressed as a phase shift with respect to it, i.e.

$$Z_4 = jtan\theta_{abc} \tag{5}$$

where $a, b, c = o, s, p$ and θ is the phase angle.

As pointed out by Zhao, what is relevant here are really the gap impedances when the output port is terminated in a load. One would want to know the induced voltage due to a bunched beam as it traverses a gap. Using Eq. (2) to eliminate V_4 and I_4 from Eq. (1) results in

$$V_i = \sum_j \zeta_{ij} I_i \tag{6}$$

where $i, j = 1, 2, 3$ only. The gap impedances ζ_{ij} are given by

$$\zeta_{ij} = Z_{ij} + \frac{Z_{i4} Z_{j4}}{Z_4 - Z_{44}} \tag{7}$$

Generally, the load at the output waveguide is matched, i.e.

$$Z_4 = -1 \tag{8}$$

with the sign consistent with the current flow convention. Then Eq. (7) simplifies to

$$\zeta_{ij} = Z_{ij} - Z_{i4} Z_{j4}. \tag{9}$$

It is worth noting that the gap impedance consists of the usual circuit impedance term plus a term due to the coupling to the output port. With the circuit impedance previuosly determined, the gap impedances are easily calculated. As an example, Table I shows the measured phase shifts for the 2π mode which lead to the determination of the impedance matrix while Table II shows the gap impedances calculated from it. The gap impedances for the $2\pi/3$ and π mode are also found in a similar way.

$$\begin{aligned}
\theta_{ooo} &= 0° \\
\theta_{soo} &= 131.5° \\
\theta_{oso} &= 102.8° \\
\theta_{oos} &= 86.2° \\
\theta_{sso} &= 103.8° \\
\theta_{sos} &= 86.2° \\
\theta_{oss} &= 86.2° \\
\theta_{poo} &= 5.525° \\
\theta_{opo} &= 8.288° \\
\theta_{oop} &= 6.078°
\end{aligned}$$

Table 1. Measured phase shifts for the 2π mode.

$$\begin{aligned}
\zeta_{11} &= 594.58 + j526.04 \\
\zeta_{22} &= 940.90 + j213.77 \\
\zeta_{33} &= 715.60 - j47.530 \\
\zeta_{12} &= 666.79 + j183.72 \\
\zeta_{13} &= 652.29 - j43.330 \\
\zeta_{23} &= 820.55 - j54.500
\end{aligned}$$

Table 2. Gap impedances for the 2π mode.

III. BEAM LOADING CONDUCTANCE

The response at a particular mode frequency of a coupled cavity chain like the three-gap output cavity, to beam excitation exhibits regions of negative beam loading conductance as the beam voltage is varied. If the absolute value of this conductance is greater than the circuit conductance, then the mode will be unstable and oscillation will occur. The circuit conductance can be directly calculated from the gap impedances determined in the previous section.

The first analytical treatment of negative beam loading in coupled-cavity chain was due to Wessel-Berg[3] who formulated the beam loading admittance for extended interaction cavities. Following his approach, the beam loading conductance of the three-gap cavity is derived and given by

$$\frac{G_b}{G_o} = -\frac{1}{8}\frac{k_e}{k_q}\left[M^2(k_e+k_q) - M^2(k_e-k_q)\right]\left[\frac{2}{\gamma(\gamma+1)}\right] \tag{10}$$

where it is normalized by the DC beam conductance

$$G_o = \frac{I_{beam}}{V_{beam}}.$$

In Eq. (10), $M(k_e+k_q)$ and $M(k_e-k_q)$ denote the coupling coefficients of the slow and fast space charge waves respectively. The definitions for the other parameters are

$$k_e = \frac{\omega}{v_e},$$
$$k_q = \frac{\omega_q}{v_e};$$

ω_q is the reduced plasma frequency, v_e is the beam velocity and γ is the usual relativistic factor. In terms of the coupling coefficient for a single gap M_g, one can write

$$M(k) = M_g(k)\sum_n A_n e^{jkz_n}/\sum_n |A_n| \tag{11}$$

where the single-gap coupling coefficient is

$$M_g(k) = \left[J_0^2\left(\frac{kd}{2}\right)\left(\frac{I_0^2(\kappa r_b) - I_1^2(\kappa r_b)}{I_0^2(\kappa r_a)}\right)\right]^{\frac{1}{2}} \tag{12}$$

In Equation (11), n is the number of gaps, A_n is the voltage amplitude and z_n is the position of the gap relative to the center of the cavity. In Equation (12), d is the gap width, r_b is the beam radius, r_a is the drift-tube radius, and

$$\kappa = (k^2 - k_0^2)^{\frac{1}{2}}.$$

From a knowledge of the relative amplitudes and directions of the fields in each gap and the parameters of the tube such as frequency, voltage and current, the beam loading conductance can be evaluated. One is to be reminded that the analysis is valid for symmetric modes only.

Fig. 3 shows the beam loading conductances of the three lowest modes calculated as a function of the beam voltage and the regions of negative beam loading are quite evident, especially for the $2\pi/3$ and 2π modes at high beam voltages. Comparing the maximum negative value of each mode over the voltage range with their repective circuit conductance calculated previously, one finds that the circuit conductance is greater in each case. As a result, one can conclude that all three modes should not oscillate.

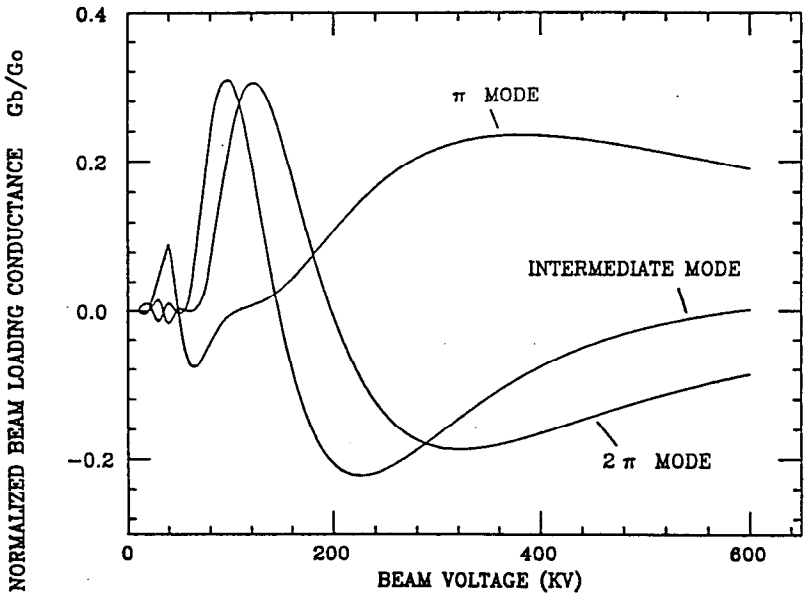

Figure 3. Normalized beam loading conductance vs beam voltage.

IV. COMPARISON OF COLD TEST AND ARGUS SIMULATIONS

Although the modes in the lowest pass band have been demonstrated to be stable, higher order modes might still oscillate if they are excited by the beam but are trapped. Such modes, if any, can be detected in most cases by cold test measurements since they would exhibit high Q_{ext}, unless they are masked by degenerate modes with low Q_{ext}'s. Experimentally, it is also difficult to identify these higher order modes, therefore numerical modeling becomes necessary.

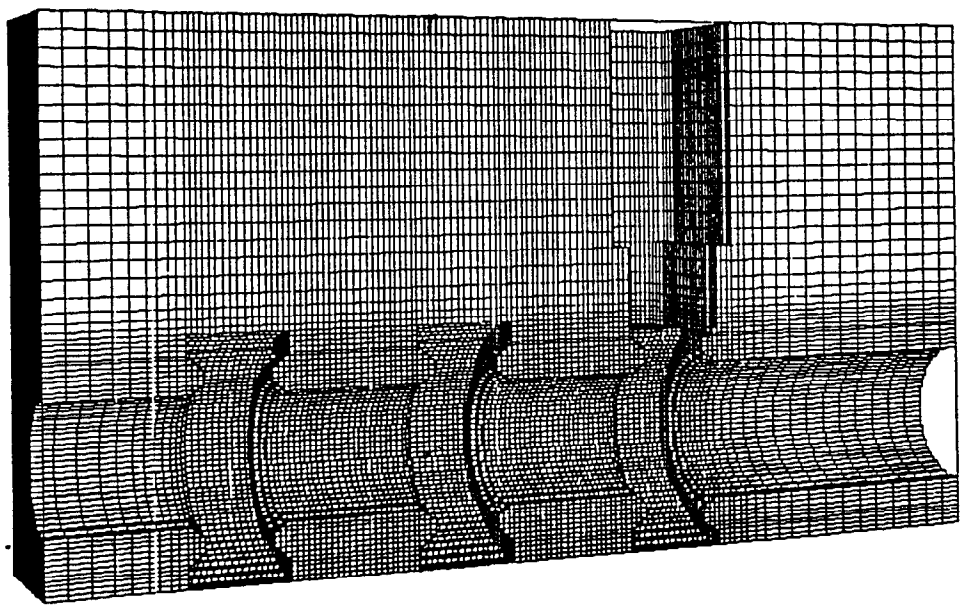

Figure 4. ARGUS model of the three-gap output cavity.

The geometry of the three-gap output cavity as modeled by ARGUS is shown in Fig. 4. The code calculates the mode spectrum for the closed cavity when the output waveguide is terminated by a short at a selectable distance L from the cavity output iris. Both the frequency and the patterns of the modes depend upon the shorting distance L. Computations were carried out for three different values of L. From these computations one can determine the oscillation frequency and Q_{ext} which would ensue for each of these modes when the waveguide is terminated by a matched load. The method of Kroll and Lin (KL)[8] was used for this purpose. Because the π and $2\pi/3$ modes were separated in frequencies by an amount comparable to their resonance widths a two resonance of the KL method was also used, but no significant modification occurred. A two resonance version of the Kroll-Yu (KY)[9] method was also applied and agreement with the KL method was found. (A fourth length in an ARGUS run would have been required to apply the single resonance KY method.) Once the oscillation frequency and Q_{ext} are determined, the KY single resonance formula enables one to compute the shorting distance L which will yield the same frequency in a computer simulation. The field pattern obtained with this choice of length, which is expected to agree closely with that which one would obtain when the waveguide is terminated by a matched load, is shown in Fig. 5. Considerable asymmetries can be observed. This indicates that further modification on the cavity is necessary to reduce any deleterious effect on the beam.

In the cold test, the resonance parameters were determined by carrying out VSWR measurements versus frequency by looking into the output waveguide. The results were in good agreement with the computer calculations, as shown in Table 3. Thus far only modes in the lowest pass band have been examined in detail. Similar analysis for the higher-order modes are in progress. Initial cold test data gives indications of potentially trapped modes. ARGUS simulations show that for modes at the same frequency range, the fields are not cut off in the enlarged downstream beam pipe. Whether or not this is the cause for certain modes to be trapped is presently under investigation.

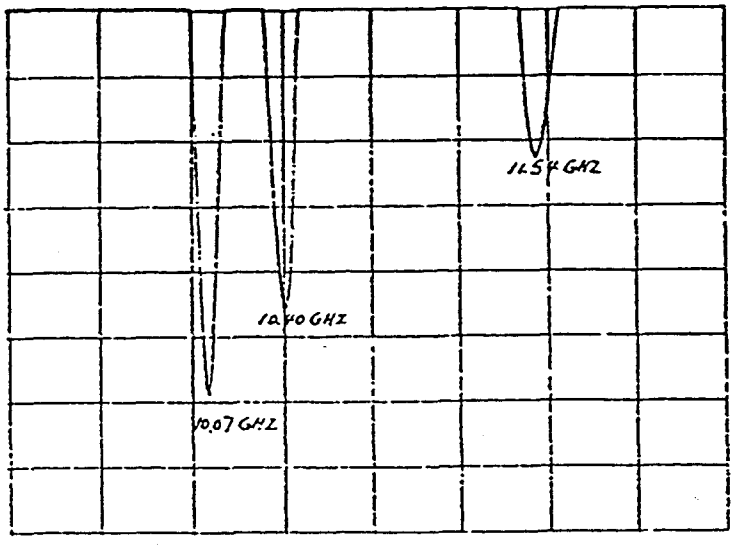

Freq. in GHz (Q_L)	π	$2\pi/3$	2π
Measured	10.07 (47)	10.40 (45)	11.54 (19)
Calculated	10.05 (45)	10.33 (44)	11.53 (20)

Table 3. Comparison of cold test data with Argus results.

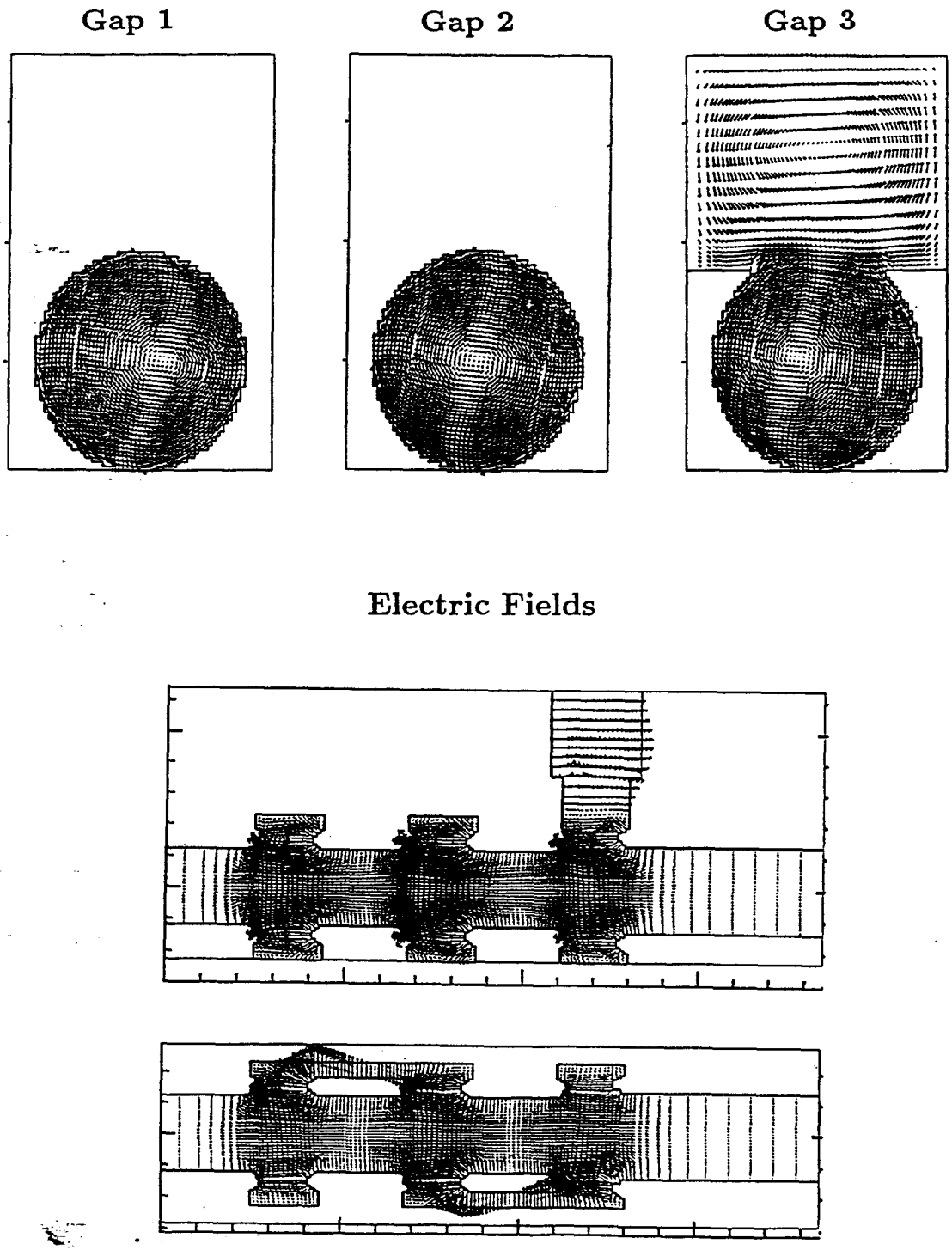

Figure 5. Field pattern for the 2π operating mode.

V. SURFACE GRADIENT AND CONVERSION EFFICIENCY

Aside from stability considerations the overriding concern in designing the output circuit is how well the two objectives of low surface gradient and high efficiency are met. Ideally, one would like to evaluate the beam interaction with the full 3-D geometry of the circuit as shown in Fig. 4. This kind of modeling, however, is not feasible at present. Instead a simpler axisymmetric 2-D (r, z) geometry is considered. In this approximation, the $2\frac{1}{2}$-D code CONDOR has been used extensively to study klystron interaction by modeling all the cavities with ports. The output cavity is then represented by a set of ports coupled together through the gap impedances derived previously. This description is valid if the actual fields in the cavity are close to being axisymmetric which as evident in Fig. 5, may not necessarily be the case.

The results from a typical CONDOR simulation are summarized in Table 4. The modeling covers the entire klystron circuit which includes the input cavity, two gain cavities, a penultimate cavity and the three-gap output cavity. All except the output cavity have single gaps so gaps 5, 6 and 7 refer to the three gaps of the output. Figure 6 and Fig. 7 plots respectively the electron position and the RF beam current along the circuit. They serve to show the bunching process occuring at the first four cavities as well as the power extraction at the output gaps.

Gap No.	Gap Volts	Axis Volts	$I_{induced}$	RF Beam P_{out}
1	7.660e+02	1.029e+03	1.364e-01	-1.664e+01
2	1.409e+04	1.898e+04	3.127e-01	5.567e+02
3	1.398e+05	1.885e+05	3.485e+01	1.070e+05
4	1.438e+05	1.939e+05	3.660e+02	1.421e+05
5	3.596e+05	4.847e+05	4.122e+02	3.115e+07
6	3.676e+05	4.954e+05	3.817e+02	6.957e+07
7	2.973e+05	4.004e+05	1.837e+02	2.827e+05

Total Power Out = 1.010e+08

Electronic Efficiency = 4.664e-01

Table 4. CONDOR simulation results for a 5-cavity klystron.

As mentioned previously, the output circuit is designed to produce 100 MW of peak power at 11.4 GHz, with a pulse width of 1 μsec at 120 pps. The results in Table 4 show over 100 MW power generation and a reasonable conversion efficiency $\sim$ 46%. However, the RF gap voltages induced by the beam are too high to be acceptable. Using the gap voltages of 360, 368 and 297 KV to scale with SUPERFISH results for a similar gap geometry one finds peak surface gradients of 1.10, 1.13 and 0.91 MV/cm respectively. These values are higher than those in the two-gap case. This seems to suggest that high efficiency and low gradients may not always be compatible design goals. Generally speaking, the higher the value of the gap impedance, the higher the efficiency, but the resulting gap fields are often too excessive. A lower value of gap impedance gives a safer gradient, but at the expense of a desirable efficiency. Currently several options are being pursued to lower the gap voltages. One can increase the coupling between the output waveguide and the cavity, one can modify the resonant frequencies of each individual cell or one can vary the spacing between cells.

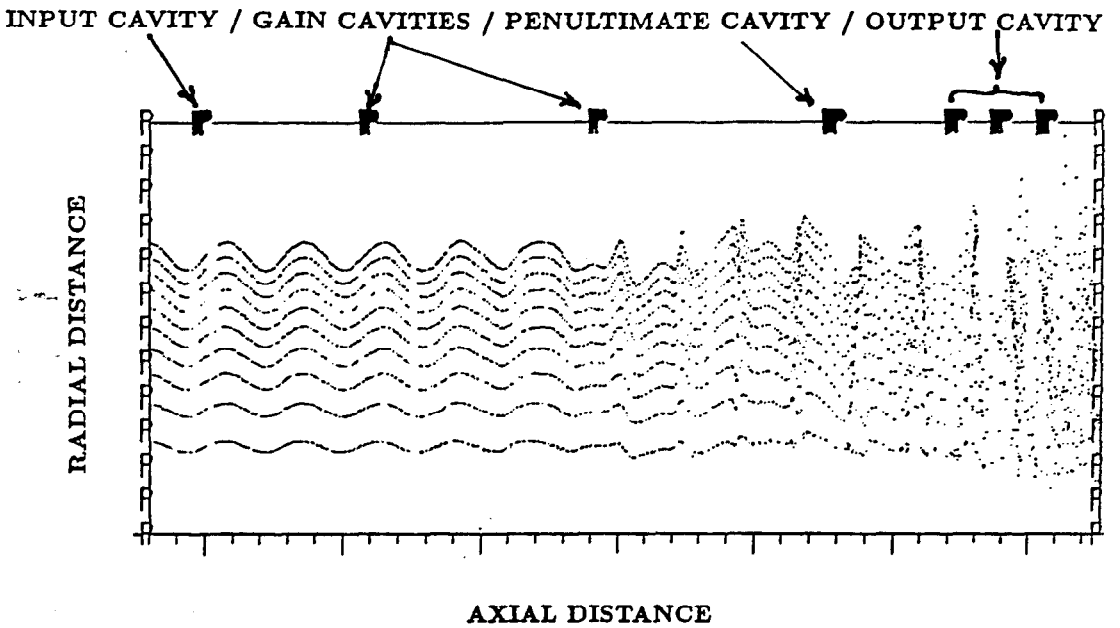

Figure 6. Electron position from CONDOR.

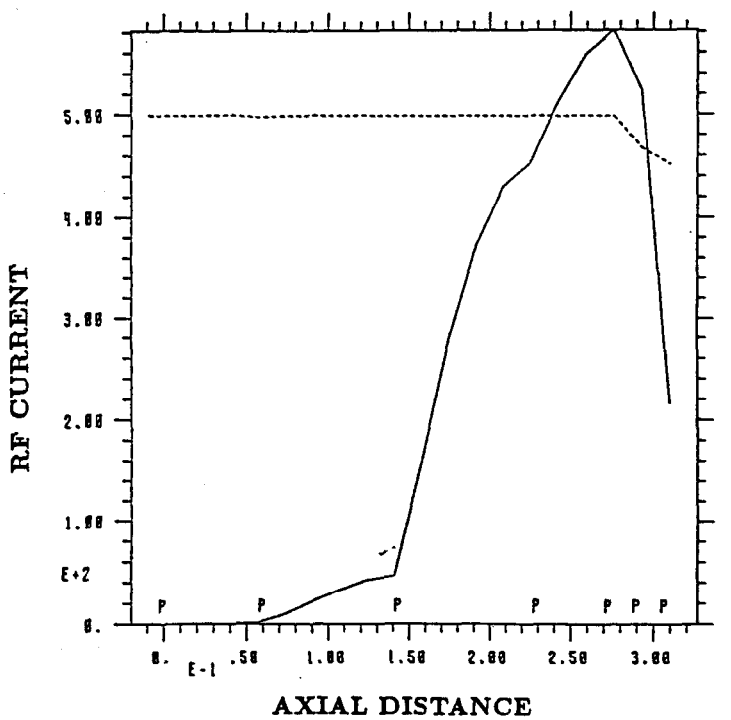

Figure 7. RF beam current vs distance

VI. CONCLUSION

A three-gap output cavity has been examined for mode stability and for power handling and extraction capabilities. The analytical and experimental methods employed in evaluating the mentioned circuit properties are described. The present design is found to satisfy power output requirement but the induced gap voltages are higher than desired. Also, the enlarged drift tube appears to be a potential cause for higher-order mode oscillations. Improvements on the circuit to reduce the gap voltages, to make the power output from each gap more equal as well as to suppress mode instability, are in progress.

ACKNOWLEDGMENT

Thanks are due to K. Eppley for implementing the circuit model for the output cavity into CONDOR.

REFERENCES

1. M. Allen et. al., "RF Power Sources for Linear Colliders," SLAC-PUB-5274 (June 1990), published in *Proceedings of the 2nd European Particle Accelerator Conference* (Nice, France, 1990).

2. G.A. Loew, Linear Collider Workshop, Protvino, USSR, 1991.

3. T. Wessel-Berg, "A General Theory of Klystrons with Arbitrary, Extended Interaction Fields," Microwave Lab., Stanford Univ., Stanford, Calif., Tech. Rep. 376, Mar. 1957.

4. A. Karp and G. T. Hunter, "Higher Order Modes and Instabilities in Coupled TWT's," *IEEE Trans. on Electron Devices*, ED-33, 1890 (1986).

5. Y. Zhao, "An Impedance Measurement Method for Double-Gap Klystron Cavity," *IEEE Trans. on Electron Devices*, ED-29, 316 (1982).

6. K. Ko et. al., " A Three-dimensional Electromagnetic Eigenvalue Solver Compatible with ARGUS," published in *Proceedings of 12th Conf. on the Numerical Simulation of Plasmas*, (San Francisco, Calif., 1987).

7. B. Aimonetti et. al., *CONDOR User's Manual*, Livermore Computing Systems Document, Lawrence Livermore National Laboratory, Livermore, Calif., April, 1988.

8. N. Kroll and X. Lin, "Efficient Computer Determination of the Properties of Waveguide Loaded Cavities," SLAC-PUB-5296 (July 1990), published in *Proceedings of the 1990 Linear Accelerator Conference* LA-12004-C, 738-740, (Los Alamos, New Mexico, 1991).

9. N. Kroll and D. Yu, "Computer Determination of the External Q and Resonant Frequency of Waveguide Loaded Cavities," *Particle Accelerators* 34, 231 (1990).